Losses Minimization Control for an Integrated Multi-Drives Topology devoted to Hybrid Electric Vehicles

G. Nobile, G. Scelba, M. Cacciato, G. Scarcella
Department of Electrical, Electronics Engineering and Computer Science
University of Catania
Catania - Italy
giovanni.nobile@dieei.unict.it

***Abstract*—This paper deals with the study and implementation of a losses minimization control method for an integrated multi-drives topology used to interface a multi windings induction machine to more storage units in hybrid electric vehicle parallel drivetrains. The main target is to optimize the management of multi-directional power flows, by reducing the power losses in the induction machine as well as in each energy storage units. The proposed control strategy continuously searches for the best compromise among the torque demand, the power capability of each storage unit and the overall power losses. In such a way, a significant improvement in the overall efficiency is obtained. Simulations and experimental tests confirm the effectiveness of the proposed method.**

Keywords—multi-drives; efficiency improving; hybrid energy storage; hybrid electric vehicles; induction machine.

I. INTRODUCTION

The reduction of power losses in electrical machines and storage systems used in parallel drivetrain of hybrid electric vehicles (HEV) is a key issue in automotive applications [1-3].

In some cases the storage system is hybrid and can include two different storage unit technologies, for instance supercapacitors and batteries. In conventional Hybrid Energy Storage Systems (HESS) for HEV, the storage units can be connected to a common DC bus by means of DC/DC converters. However, such configuration implies some disadvantages, in terms of system reliability and stability, [1].

Efficiency of the power conversion process directly impacts on the vehicle range. Some contributions focused on the development of losses minimization control strategies have been proposed in past literature. The analyses are mainly focused on the electric machine, while a comprehensive losses evaluation including the storage units has not been provided yet [4-6].

In this paper a losses minimization control for an integrated multi-drives (IMD) topology devoted to HEVs is presented, exploiting a multi winding induction machine. A suitable modeling of supercapacitors and batteries allows to establish in a simple and effective way the vector control strategy required to control the sub-units composing the electrical machine, complying with some technical constraints in terms of power capability assessment and manufacturer recommendations affecting the State of Health (*SOH*) of the storage units while minimizing the overall power losses.

II. SYSTEM MODELING

The IMD configuration considered in this paper has been presented in [7].

The conventional winding of a standard squirrel cage induction machine is split into different three-phase sub-windings, keeping the same original mmf distribution, as shown in Fig. 1. Each winding has a different number of turns N_j depending on the desired back emf. The wires cross section is related to the rated current.

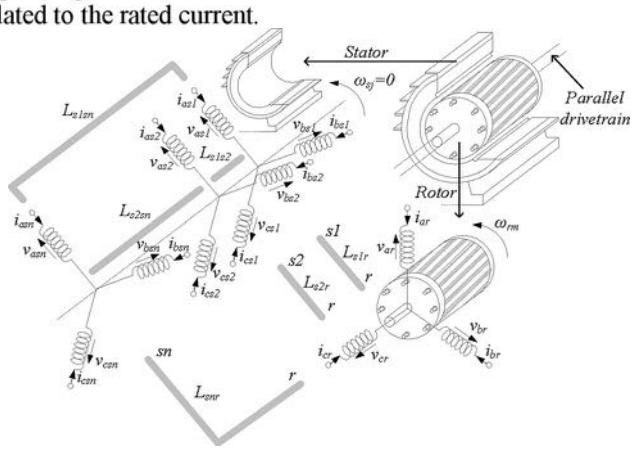

Fig. 1. Schematical representation of the three-phase sub-machines.

The total magnetic airgap flux and the torque generated in the electromagnetic system can be approximated (under the assumption of linear system) as the sum of the contributions provided by each fictitious sub-machine (SM), each one consisting of one of the sub-windings and sharing the same rotor. This electromagnetic system allows to supply different storage units featuring different power capabilities and DC voltage levels by means of standard three-phase voltage source inverters (VSI), each one connected to a single SM.

The same *qd* reference frame must be used for all the drives. According to [7], the IMD can be easily controlled by implementing n decoupled field oriented control (FOC) algorithms in the SMs. The field orientation is obtained by imposing the total slip angular frequency $\omega_{s\lambda r}$ equal to:

$$\omega_{s\lambda r} = \frac{1}{\tau_r} \cdot \frac{\left(i_{qs1} + i_{qs2} \cdots + i_{qsn}\right)}{\left(i_{ds1} + i_{ds2} \cdots + i_{dsn}\right)} \tag{1}$$

where τ_r is the rotor time constant, while i_{qsj} and i_{dsj} are the torque and flux components of the stator current vectors flowing in the *j-th* SM. It is worth noting that in this analytical formulation the electrical quantities associated to the *j-th* stator winding (and to the rotor) are referred to the reference stator winding 1 through the turns ratio N_1/N_j (N_1/N_r for the rotor). The rotor flux angular position $\theta_{\lambda r}$ is calculated from $\omega_{s\lambda r}$ and from the rotor speed ω_{re} as:

$$\theta_{\lambda r} = \theta_{\lambda r0} + \int \left(\omega_{s\lambda r} + \omega_{re}\right) dt \tag{2}$$

The electromagnetic torque provided by the IMD can be expressed as the sum of the torque contributions provided by each SM:

$$\begin{aligned} T_e &= \frac{P_m}{\omega_{rm}} = \frac{3}{2}\overline{p}\left(i_{qs1} + ... + i_{qsn}\right)\lambda'_{dr} = \\ &= \frac{3}{2}\overline{p}L_M\left(i_{qs1} + ... + i_{qsn}\right)\cdot\left(i_{ds1} + ... + i_{dsn}\right) = \\ &= T_{e1} + ... + T_{en} \end{aligned} \tag{3}$$

where:

$$T_{ej} = \frac{3}{2}\overline{p}L_M i_{qsj}\left(i_{ds1} + ... + i_{dsn}\right) \tag{4}$$

Therefore, under field orientation, the torque produced by the n integrated motors is proportional to the algebraic sum of the torque components i_{qsj}. Likewise, the amplitude of the flux is given by the algebraic sum of the flux components i_{dsj}.

Fig. 2 displays a block diagram of the IFOC implemented in the *j-th* SM. The current loop allows to perform the decoupled torque and flux control in each SM. The reference currents must be assigned in order to improve the overall efficiency considering the operating scenario (braking, cranking, etc.) and the state of storage units, as detailed in the following.

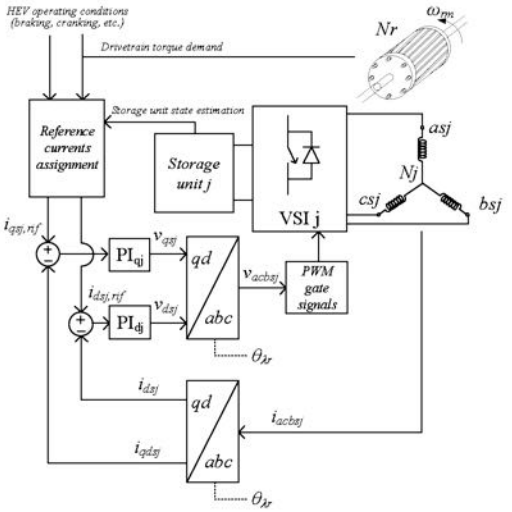

Fig. 2. Block diagram of the IFOC used for the *j-th* SM in the IMD system.

The storage units used in HEV parallel drivetrains, represented by strings of supercapacitors and series-connected batteries (both lead-acid and lithium-ions technologies), have to be appropriately modeled in order to reach a good accuracy in the estimation of their *SOC* and power capability *PC*. Indeed, these parameters are crucial to assess the suitable energy management for the entire IMD system.

The most straightforward approach to model the supercapacitors strings (*sc*) is to consider a simple RC network constituted by the series of a capacitor C_{sc} and of a resistor ESR_{sc}, as proposed by several authors and supercapacitors manufacturers, [8]. The parameters C_{sc} and ESR_{sc} can be easily identified using data provided by the manufacturer of the supercapacitor cells:

$$\begin{aligned} C_{sc} &= C_{sc,cell} / n_{sc} \\ ESR_{sc} &= ESR_{sc,cell} \cdot n_{sc} \\ v_{sc} &= v_{sc,cell} \cdot n_{sc} \\ v_{sc,rated} &= v_{sc,cell,rated} \cdot n_{sc} \end{aligned} \tag{5}$$

where n_{sc} is the number of series-connected supercapacitors.

The actual state of charge of the supercapacitor SOC_{sc} is the ratio between the actual voltage v_{sc} and the maximum voltage $v_{sc,max}$ [2]:

$$SOC_{sc} = \frac{v_{sc}}{v_{sc,max}} \tag{6}$$

Generally, the maximum value of voltage is assigned equal to the rated one. Moreover, during normal operation the SOC_{sc} is usually maintained between 35-40% ($SOC_{sc,min}$) and 95% ($SOC_{sc,max}$) [1]. The power capability of the supercapacitor during the discharge process is function of the actual SOC_{sc} and of the selected horizon time Δt depending on the actual operating scenario of the drivetrain (acceleration, engine cranking, etc.) [9]:

$$PC_{sc,ds} = i_{sc,ds,PC} \cdot \left(SOC_{sc} - \left| \frac{SOC_{sc} - SOC_{sc,min}}{2} \right| \right) \cdot v_{sc,max} \tag{7}$$

where $i_{sc,ds,PC}$ is the maximum value of the current that can be imposed during the discharge process considering the actual SOC_{sc} and the minimum $SOC_{sc,min}$ that can be reached:

$$i_{sc,ds,PC} = \frac{SOC_{sc} - SOC_{sc,min}}{\Delta t} v_{sc,max} \cdot C_{sc} \tag{8}$$

A similar formulation can be reported for the charge process.

Differently than modeling of supercapacitors, modeling of batteries (*bt*) is more complicated due to several non-linear phenomena occurring during charge and discharge. The accurate estimation of SOC_{bt} is often a difficult task [10]. In this study the battery pack has been modeled with the equivalent electric circuit represented in Fig. 3 [11]. In the latter circuit you can note the dependency of the no-load voltage E_0 and of the internal resistance R_i from actual SOC_{bt}. The parameters R_t and C_t are used to describe the battery dynamic behavior [12].

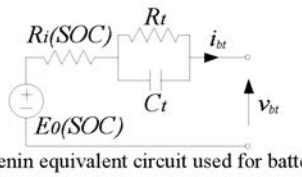

Fig. 3. Thevenin equivalent circuit used for battery modeling.

The parameters of this battery circuital representation can be identified as reported in [13]. The estimation of SOC_{bt} is performed by using the PI-based observer scheme presented in [13]. A good accuracy in power capability prediction can be obtained by means of specific algorithms, such as the one in [14] that takes into account the rate limits on actual SOC_{bt}. The value of power that can be continuously delivered without exceed

SOC_{bt} limits during a discharge, considering a given time horizon Δt, can be predicted as:

$$PC_{bt,ds} = v_{bt,min} \cdot i_{bt,ds,PC} \tag{9}$$

$$i_{bt.,ds,PC} = \frac{SOC_{bt} - SOC_{bt,min}}{\Delta t} \cdot SOH \cdot C_{bt} \tag{10}$$

C_{bt} is the rated capacity of the battery. A similar formulation can be reported about the charge process but, due to additional phenomena, it is often introduced an efficiency index, [15]. Another constraints regarding the charge process is related to the charge current recommended by the battery manufacturer pursuing the objective to extend lifetime. The selected charge current is usually lower with respect to the one calculated from PC assessment i.e. $i_{bt,ch} < i_{bt,ch,PC}$.

In the following study some of the main HEV operating scenarios are shown in Figs 4-7 considering an IMD consisting of two SMs and thus including two storage units: (1) a battery pack and (2) a string of supercapacitors. By assuming that the IMD is operated at rated flux conditions, the electromagnetic torque equation provides a linear relationship between the q-axis current components:

$$i_{qs1} + i_{qs2} = \frac{T_{e,demand}}{\frac{3}{2}\overline{p}L_M\left(i_{ds1,rated} + i_{ds2,rated}\right)} \tag{11}$$

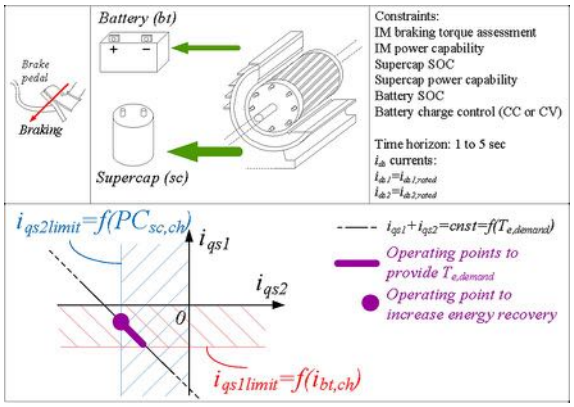

Fig. 4. Braking scenario.

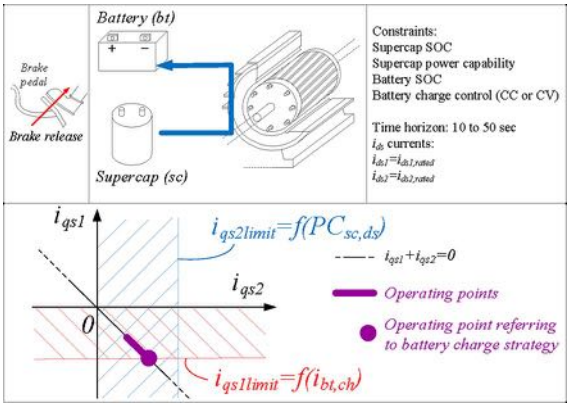

Fig. 5. Brake release scenario.

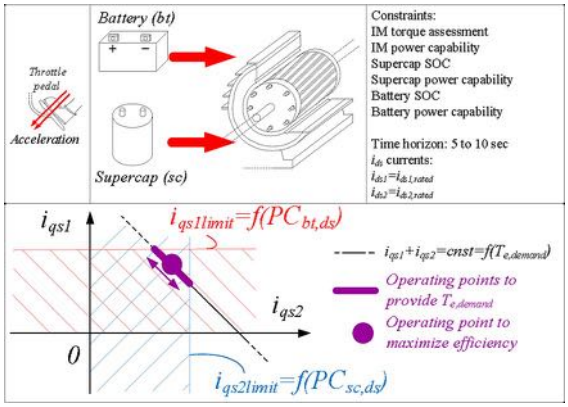

Fig. 6. Acceleration scenario.

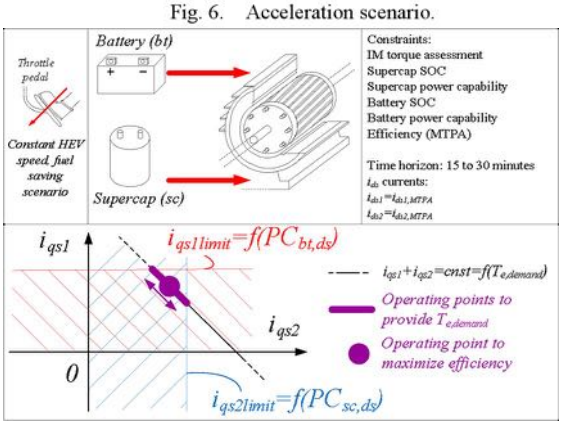

Fig. 7. Constant HEV speed, fuel saving scenario.

Moreover, according to the above mentioned constraints associated to the storage technologies, for each working scenario of the HEV, the range of operation of the drive is a portion of the straight line highlighted in the figures. Hereafter, the optimal combination of i_{qs1} and i_{qs2} have to be chosen in order to minimize the system losses.

III. Losses Estimation and Minimization

A suitable control strategy can be implemented in order to minimize the overall power losses while being compliant to the constraints related to each operating scenario.

By neglecting the losses associated to the power converters, the total power losses $\sum P_l$ in the IMD can be expressed as:

$$\sum P_l = P_{l,sc} + P_{l,bt} + P_{js1} + P_{js2} + P_{jr} + P_{fe} \tag{12}$$

The power loss $P_{l,sc}$ are Joule losses associated to the internal resistance ESR_{sc} of the supercapacitor:

$$P_{l,sc} = ESR_{sc} \cdot i_{sc}^2 \tag{13}$$

According to the experimental results shown later, the mathematical relationship between the supercapacitor current i_{sc} and the i_{qs2} current is a quasi-linear function. Such relation can be approximated by means of a constant K_{sc}:

$$i_{sc} = K_{sc} \cdot i_{qs2} \tag{14}$$

$$P_{l,sc} = ESR_{sc} \cdot K_{sc}^2 \cdot i_{qs2}^2 \tag{15}$$

Also the losses associated to the battery packs can be evaluated by considering Joule losses on resistive elements:

$$P_{l,bt} = \left(R_i(SOC) + R_t\right) \cdot i_{bt}^2 \tag{16}$$

The resistance value R_i is depending on SOC_{bt}, [13]. Anyway, since the most operating scenarios take place in a short time interval, the SOC_{bt} variation is not significant, hence it can be assigned a constant value for R_i on the basis of the initial SOC_{bt}. Similarly to supercapacitors, the mathematical relation between the battery current i_{bt} and the i_{qs1} current is a quasi-linear function. Such relation can be approximated by means of a constant K_{bt}:

$$i_{bt} = K_{bt} \cdot i_{qs1} \tag{17}$$

$$P_{l,bt} = (R_i + R_t) \cdot K_{bt}^2 \cdot i_{qs1}^2 = R_{bt} \cdot K_{bt}^2 \cdot i_{qs1}^2 \tag{18}$$

The copper losses in the stators of both the SMs can be calculated as:

$$P_{js1} = 3 \cdot R_{s1} \cdot I_{as1}^2 = \frac{3}{2} \cdot R_{s1} \cdot (i_{qs1}^2 + i_{ds1}^2) \tag{19}$$

$$P_{js2} = 3 \cdot R_{s2} \cdot I_{as2}^2 = \frac{3}{2} \cdot R_{s2} \cdot (i_{qs2}^2 + i_{ds2}^2) \tag{20}$$

Because of the rotor flux orientation imposed by the control approach, the copper losses in the rotor can be approximated as, [4], [16]:

$$P_{jr} \cong \frac{3}{2} \cdot R_r \cdot I_{qr}^2 = \frac{3}{2} \cdot R_r \cdot \frac{L_M^2}{L_r^2} \cdot \left(i_{qs1} + i_{qs2}\right)^2 \tag{21}$$

By neglecting the iron losses in the rotor, P_{fe} representing the iron losses in the stator, can be expressed as, [17-19]:

$$P_{fe} \cong P_{fes} \tag{22}$$

$$P_{fes} \cong \frac{\omega_e^2 \cdot \lambda_m^2}{R_{fe}} \tag{23}$$

in which λ_m is the airgap flux. The field orientation condition leads to:

$$\begin{cases} \lambda_{qm} \cong 0 \\ \lambda_{dm} \cong \lambda_{dr} \end{cases} \tag{24}$$

so that:

$$P_{fe} \cong \frac{\omega_e^2 \cdot \lambda_{dr}^2}{R_{fe}} \tag{25}$$

$$\lambda_{dr} = L_{lr} \cdot i_{dr} + L_M \cdot i_{dm} \tag{26}$$

This formula can be approximated as:

$$\lambda_{dr} = L_{lr} \cdot (i_{ds} - i_{dm}) + L_M \cdot i_{dm} \cong L_{lr} \cdot i_{ds} + L_M \cdot i_{dm} \tag{27}$$

in which the product $L_{lr} \cdot i_{dm}$ has been neglected. From [18] the current i_{dm} is biven by:

$$i_{dm} = \frac{L_r \cdot \left(\lambda_{dr} + L_r \cdot L_{lr} \cdot i_{ds}\right) + \dfrac{\omega_e \cdot L_M \cdot L_{lr}^2 \cdot i_{qs}}{R_{fe}}}{K_\delta} \tag{28}$$

$$K_\delta = \frac{\omega_e^2 \cdot L_M^2 \cdot L_{lr}^2}{R_{fe}^2} + L_r^2 \tag{29}$$

Therefore, the flux λ_{dr} can be expressed as:

$$\lambda_{dr} = L_{lr} \cdot i_{ds} + \frac{L_M \cdot L_r \cdot \lambda_{dr}}{K_\delta} + \frac{L_M \cdot L_r \cdot L_{lr} \cdot i_{ds}}{K_\delta} + \\ + \frac{\omega_e \cdot L_M^2 \cdot L_{lr}^2}{R_{fe} \cdot K_\delta} \cdot i_{qs} \tag{30}$$

The contribution of i_{qs} in (30) is negligible. Hence, P_{fe} can be expressed as:

$$P_{fe} \cong \frac{\omega_e^2 \cdot \lambda_{dr}^2}{R_{fe}} = \frac{\omega_e^2}{R_{fe}} \cdot \left(K_\alpha \cdot i_{ds} + K_\beta \cdot i_{qs}\right)^2 = \\ = \frac{\omega_e^2}{R_{fe}} \cdot \left(K_\alpha^2 \cdot i_{ds}^2 + K_\beta^2 \cdot i_{qs}^2 + 2 \cdot K_\alpha \cdot K_\beta \cdot i_{ds} \cdot i_{qs}\right) \tag{31}$$

where:

$$K_\alpha = \frac{\left(L_{lr} + \dfrac{L_M \cdot L_r \cdot L_{ls}}{K_\delta}\right)}{\left(1 - \dfrac{L_M \cdot L_r}{K_\delta}\right)} \qquad K_\beta = \frac{\dfrac{\omega_e \cdot L_M^2 \cdot L_{lr}^2}{R_{fe} \cdot K_\delta}}{\left(1 - \dfrac{L_M \cdot L_r}{K_\delta}\right)} \tag{32}$$

The power loss P_{fe} can be rewritten as a function of the currents i_{qs1}, i_{qs2}, i_{ds1} and i_{ds2}, by considering the current relationships of (33):

$$i_{qs} = i_{qs1} + i_{qs2} \\ i_{ds} = i_{ds1} + i_{ds2} \tag{33}$$

$$P_{fe} = \frac{\omega_e^2}{R_{fe}} \cdot K_\alpha^2 \cdot i_{ds1}^2 + \frac{\omega_e^2}{R_{fe}} \cdot K_\alpha^2 \cdot i_{ds2}^2 + 2 \cdot \frac{\omega_e^2}{R_{fe}} \cdot K_\alpha^2 \cdot i_{ds1} \cdot i_{ds2} \\ + \frac{\omega_e^2}{R_{fe}} \cdot K_\beta^2 \cdot i_{qs1}^2 + \frac{\omega_e^2}{R_{fe}} \cdot K_\beta^2 \cdot i_{qs2}^2 + 2 \cdot \frac{\omega_e^2}{R_{fe}} \cdot K_\beta^2 \cdot i_{qs1} \cdot i_{qs2} + \\ + 2 \cdot \frac{\omega_e^2}{R_{fe}} \cdot K_\alpha \cdot K_\beta \cdot i_{qs1} \cdot i_{ds1} + 2 \cdot \frac{\omega_e^2}{R_{fe}} \cdot K_\alpha \cdot K_\beta \cdot i_{qs2} \cdot i_{ds1} + \\ + 2 \cdot \frac{\omega_e^2}{R_{fe}} \cdot K_\alpha \cdot K_\beta \cdot i_{qs1} \cdot i_{ds2} + 2 \cdot \frac{\omega_e^2}{R_{fe}} \cdot K_\alpha \cdot K_\beta \cdot i_{qs2} \cdot i_{ds2} \tag{34}$$

Finally, the formulation of the total power losses becomes:

$$\sum P_l = P_{l,sc} + P_{l,bt} + P_{js1} + P_{js2} + P_{jr} + P_{fe} = \\ = ESR_{sc} \cdot K_{sc}^2 \cdot i_{qs2}^2 + R_{bt} \cdot K_{bt}^2 \cdot i_{qs1}^2 + \frac{3}{2} \cdot R_{s1} \cdot (i_{qs1}^2 + i_{ds1}^2) + \\ + \frac{3}{2} \cdot R_{s2} \cdot (i_{qs2}^2 + i_{ds2}^2) + \frac{3}{2} \cdot R_r \cdot \frac{L_M^2}{L_r^2} \left(i_{qs1} + i_{qs2}\right)^2 + P_{fe} \tag{35}$$

The main target in this study is to identify the optimal set of *qd* currents to allow the total losses minimization. The first step is to detect the stationary points for which the gradient of total power losses is minimum. In the following analysis, the currents i_{ds1} and i_{ds2} are considered constants and equal to their rated values. The gradient of ΣP_l is given by the system:

$$\nabla \sum P_l = \begin{cases} f_{x_1} = \dfrac{\partial \sum P_l}{\partial i_{qs1}} \\ f_{x_2} = \dfrac{\partial \sum P_l}{\partial i_{qs2}} \end{cases} =$$

$$= \begin{cases} f_{x_1} = \left(2 \cdot R_{bt} \cdot K_{bt}^2 + 3 \cdot R_{s1} + 3 \cdot R_r \cdot \dfrac{L_M^2}{L_r^2} + 2 \cdot \dfrac{\omega_e^2}{R_{fe}} \cdot K_\beta^2 \right) \cdot i_{qs1} + \\ + \left(3 \cdot R_r \cdot \dfrac{L_M^2}{L_r^2} + 2 \cdot \dfrac{\omega_e^2}{R_{fe}} \cdot K_\beta^2 \right) \cdot i_{qs2} + \\ + 2 \cdot \dfrac{\omega_e^2}{R_{fe}} \cdot K_\alpha \cdot K_\beta \cdot \left(i_{ds1} + i_{ds2} \right) \\ f_{x_2} = \left(2 \cdot R_{sc} \cdot K_{sc}^2 + 3 \cdot R_{s2} + 3 \cdot R_r \cdot \dfrac{L_M^2}{L_r^2} + 2 \cdot \dfrac{\omega_e^2}{R_{fe}} \cdot K_\beta^2 \right) \cdot i_{qs2} + \\ + \left(3 \cdot R_r \cdot \dfrac{L_M^2}{L_r^2} + 2 \cdot \dfrac{\omega_e^2}{R_{fe}} \cdot K_\beta^2 \right) \cdot i_{qs1} + \\ + 2 \cdot \dfrac{\omega_e^2}{R_{fe}} \cdot K_\alpha \cdot K_\beta \cdot \left(i_{ds1} + i_{ds2} \right) \end{cases} \tag{36}$$

The solutions of (36) lead to the identification of stationary points. In order to assess if these stationary points correspond to minimum for the function $\sum P_l$, the Hessian matrix must be calculated:

$$H = \begin{vmatrix} f_{x_1 x_1} & f_{x_1 x_2} \\ f_{x_2 x_1} & f_{x_2 x_2} \end{vmatrix} = \begin{vmatrix} \dfrac{\partial f_{x_1}}{\partial i_{qs1}} & \dfrac{\partial f_{x_1}}{\partial i_{qs2}} \\ \dfrac{\partial f_{x_2}}{\partial i_{qs1}} & \dfrac{\partial f_{x_2}}{\partial i_{qs2}} \end{vmatrix} \tag{37}$$

$$\begin{aligned} f_{x_1 x_1} &= \frac{\partial f_{x_1}}{\partial i_{qs1}} = 2 \cdot R_{bt} \cdot K_{bt}^2 + 3 \cdot R_{s1} + 3 \cdot R_r \cdot \frac{L_M^2}{L_r^2} + 2 \cdot \frac{\omega_e^2}{R_{fe}} \cdot K_\beta^2 \\ f_{x_1 x_2} &= \frac{\partial f_{x_1}}{\partial i_{qs2}} = 3 \cdot R_r \cdot \frac{L_M^2}{L_r^2} + 2 \cdot \frac{\omega_e^2}{R_{fe}} \cdot K_\beta^2 \\ f_{x_2 x_1} &= \frac{\partial f_{x_2}}{\partial i_{qs1}} = 3 \cdot R_r \cdot \frac{L_M^2}{L_r^2} + 2 \cdot \frac{\omega_e^2}{R_{fe}} \cdot K_\beta^2 = f_{x_1 x_2} \\ f_{x_2 x_2} &= \frac{\partial f_{x_2}}{\partial i_{qs2}} = 2 \cdot R_{sc} \cdot K_{sc}^2 + 3 \cdot R_{s2} + 3 \cdot R_r \cdot \frac{L_M^2}{L_r^2} + 2 \cdot \frac{\omega_e^2}{R_{fe}} \cdot K_\beta^2 \end{aligned} \tag{38}$$

It can be demonstrated that in the above mathematical formulation the determinant of the Hessian matrix is positive, as well as the f_{x1x1} term. Under the constraints related to one of the operating scenarios shown in Figs 4-7, the determination of the stationary points of (36) becomes a constrained minimums formulation leading to the identification of a single set of currents $i_{qs1}{}^{\Delta}$, $i_{qs2}{}^{\Delta}$ which ensure the minimization of the total losses:

$$\min\left(\sum P_l\right) \tag{39}$$

moreover, considering the constraint:

$$i_{qs1} + i_{qs2} = constant = f(T_{e,demand}) \tag{40}$$

a simple solution can be analytically found:

$$\frac{i_{qs1}{}^{\Delta}}{i_{qs2}{}^{\Delta}} \cong \frac{i_{qs1}{}^{*}}{i_{qs2}{}^{*}} = \frac{2 \cdot R_{sc} \cdot K_{sc}^2 + 3 \cdot R_{s2}}{2 \cdot R_{bt} \cdot K_{bt}^2 + 3 \cdot R_{s1}} \tag{41}$$

which together to (40) represent a simple way to identify $i_{qs1}{}^{\Delta}$ and $i_{qs2}{}^{\Delta}$ with a good accuracy by directly calculating $i_{qs1}{}^{*}$ and $i_{qs2}{}^{*}$. Such ratio is obtained by means of suitable simplifications due to the typical magnitude of the various parameters in (36).

IV. Simulations

A preliminary validation of the proposed approach has been conducted by numerical simulations. In particular, the case study "Acceleration" is focused. The chart in Fig. 6 can be analytically formulated as:

$$\begin{cases} i_{qs1} + i_{qs2} = \dfrac{T_{e,demand}}{\dfrac{3}{2} \overline{p} L_M \left(i_{ds1,rated} + i_{ds2,rated} \right)} \\ T_{e,demand} \le T_{IM,rated} \\ i_{qs1} \le i_{qs1limit} \\ i_{qs1limit} = f(PC_{bt,ds}) \\ i_{qs2} \le i_{qs2limit} \\ i_{qs2limit} = f(PC_{sc,ds}) \end{cases} \tag{42}$$

By assuming that mechanical losses are negligible, the currents $i_{qs1limit}$ and $i_{qs2limit}$ can be calculated in a straightforward way:

$$i_{qs1limit} \quad \frac{PC_{bt,ds}}{\dfrac{3}{2} \overline{p} L_M \left(i_{ds1,rated} + i_{ds2,rated} \right) \omega_{rm,rated}} \tag{43}$$

$$i_{qs2limit} \quad \frac{PC_{sc,ds}}{\dfrac{3}{2} \overline{p} L_M \left(i_{ds1,rated} + i_{ds2,rated} \right) \omega_{rm,rated}} \tag{44}$$

In this scenario, the final speed is not known in advance. Therefore, for safety reasons, the most reasonable assumption is to consider that the final speed is equal to the rated one. The i_{ds1} and i_{ds2} currents are equal to the rated value in order to improve the dynamical behavior during transients. The energy management strategy has to establish the optimal set of currents i_{qs1}, i_{qs2} while respecting the constraints in system (42). Two possibility are available: solve the system (39) which is time consuming and depending on many parameters, or apply the formula (41), which combined to (40) provides a good approximation of the optimal operating condition, as proven in the following.

TABLE I. IMD and Storage Units: Main Technical Data

Multi Winding Induction Machine 2.2 kW			
		SM1	***SM2***
Rated Voltage (V)		266	133
Rated Frequency (Hz)		50	50
Rated speed (rpm)		1470	1470
Rated current (A)		4.86	4.86
Battery ***(n_{bt} 24 V batteries in series)***		***Supercap*** ***(n_{sc} 16 V supercapacitors in series)***	
Rated Voltage (V)	24	Rated Voltage (V)	16
Rated Capacity (Ah)	7.2	Rated Capacity (F)	9.5
n_{bt}	19	*ESR* (mΩ)	5.3
Technology	VRLA	n_{sc}	19

Technical data of the main components composing the IMD system are reported in Table I.

Fig. 8 displays the trend of electrical and mechanical quantities of a random driving cycle including the considered scenarios. For each scenario, the reference *qd* currents are calculated considering the constraints related to the actual power capability of batteries and supercapacitors.

Focusing on the scenario "Acceleration" highlighted in yellow, the actual value of currents i_{qs1} and i_{qs2} have been chosen on the basis of the constraints in Fig. 6. From Fig. 6 and from (42) the boundary currents $i_{qs1limit}$ and $i_{qs2limit}$ can be determined according to the following steps.

Starting from the knowledge of PC_{IM}=2.2 kW, $\omega_{rm,rated}$=153.9 rad/s → $T_{e,demand}$=14.3 Nm, and rated flux condition i_{ds1}= $i_{ds1,rated}$=1.84 A, i_{ds2}= $i_{ds2,rated}$=0.5 A it is possible to determine

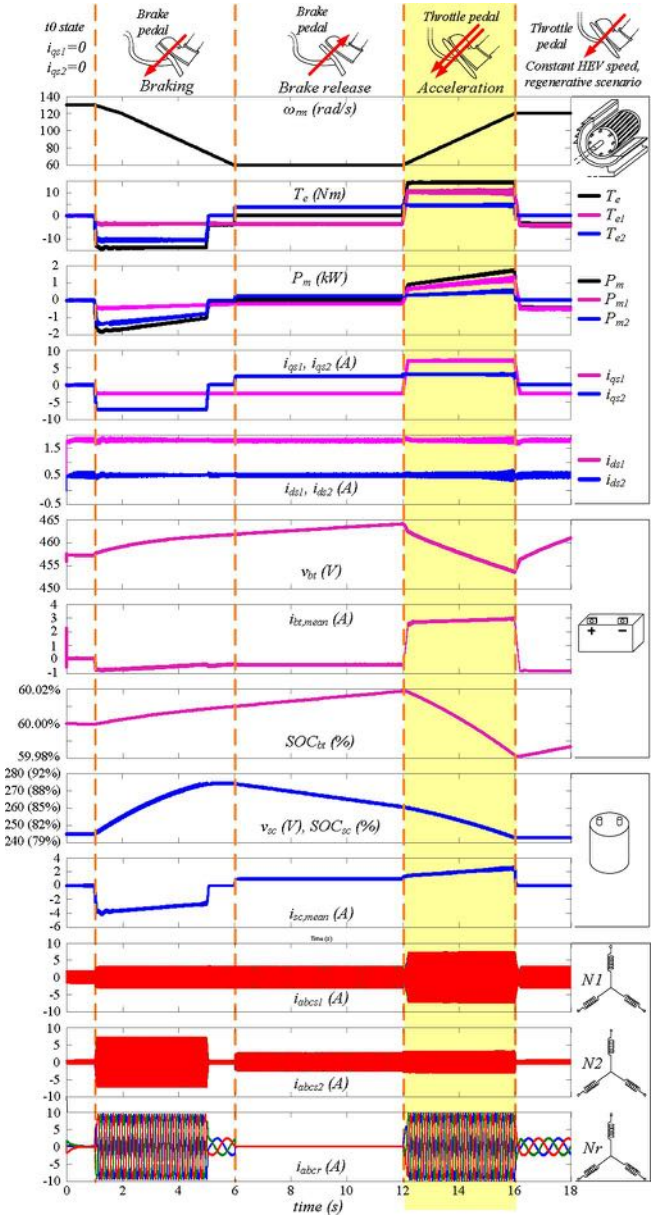

Fig. 8. Random driving cycles including the main operating scenarios. The losses minimization analysis described in this section is related to the "Acceleration" scenario highlighted in yellow.

the linear relationship between the q-axis current components:

$$T_{e,demand},\ i_{ds1},\ i_{ds2} \rightarrow i_{qs1}+i_{qs2}\approx 10\ \text{A}$$

By imposing the constraints associated to the storage units:

- Δt=10 s, $SOC_{bt,t0}$=60%, $SOC_{bt,min}$=50%, $v_{bt,min}$=380 V
- Δt=10 s, $SOC_{sc,t0}$=85%, $SOC_{sc,min}$=35% ,$v_{sc,max}$=304 V → $PC_{sc,ds}$≈1400 W

we can univocally determine the current limits: $i_{qs1limit}$>>10 A from (10) and (17), $i_{qs2limit}$≈6.5 A from (8) and (14).

The actual operating conditions have been represented in the chart of Fig. 9. Since the losses minimization is the main requirement in this study, the final target is to select a set of currents i_{qs1} e i_{qs2} ensuring the efficiency improvement together with the constraints $i_{qs1}+i_{qs2}\approx 10$ A and $i_{qs2}\le i_{qs2limit}$=6.5 A.

Evaluating the losses by means of (35), the chart of Fig. 10 has been carried out, showing the total losses as a function of i_{qs1} and i_{qs2}. The minimum point corresponds to a power loss of about 540 W obtained with the set of currents $i_{qs1}{}^{\Delta}$=6.10 A and $i_{qs2}{}^{\Delta}$=3.90 A calculated by solving (39).

Alternatively, it can be exploited the simplified approach combining (40) and (41):

$$\begin{cases} \dfrac{i_{qs1}}{i_{qs2}} \cong \dfrac{2\cdot R_{sc}\cdot K_{sc}^2+3\cdot R_{s2}}{2\cdot R_{bt}\cdot K_{bt}^2+3\cdot R_{s1}} = 1.5106 \\ i_{qs1}+i_{qs2}=10 \end{cases} \qquad (45)$$

$$i_{qs1}{}^{*}=6.02\,A,\quad i_{qs2}{}^{*}=3.98\,A$$

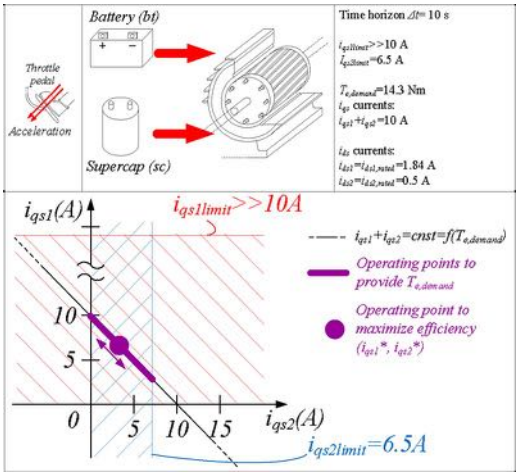

Fig. 9. "Acceleration" scenario under investigation

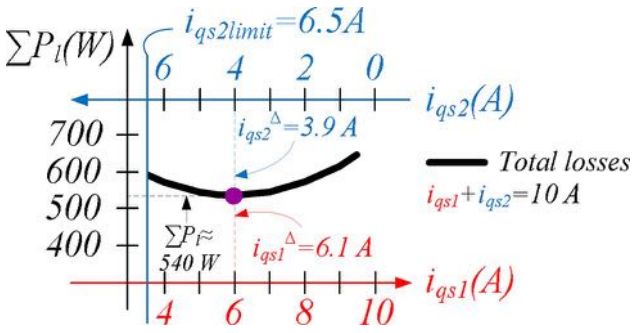

Fig. 10. Total losses curve for the "Acceleration" scenario

It is quite evident that the latter set of currents (i_{qs1}^{*}=6.02 A and i_{qs2}^{*}=3.98 A), is very close to the optimal currents coming from the comprehensive analytical formulation (i_{qs1}^{Δ}=6.10 A and i_{qs2}^{Δ}=3.90 A), with a relative error less than 2%.

V. Experimental Tests

Experimental tests have been conducted in order to verify the effectiveness of the proposed control strategy for the IMD used even in the simulations, whose technical data are summarized in Table I. The storage unit 1 is a 120 V 27 Ah VRLA battery pack, while the storage unit 2 consists of a 84 V 27 Ah VRLA battery pack. The drivetrain is mechanically coupled to a 4 kW induction motor drive in which an IFOC is implemented to impose the operating speed profile. The power losses are measured during the experimental tests by using digital power meters.

Experimental tests have been focused on the "Braking" scenario depicted in Fig. 4, in which the storage units can be recharged through the regenerative power coming from the mechanical system.

The sum $i_{qs1} + i_{qs2}$ is strictly related to the required braking torque $T_{e,demand}$, while $\omega_{rm,t0}$ represents the initial rotor speed at the beginning of the braking.

The boundary currents $i_{qs1limit}$ and $i_{qs2limit}$ are functions of the maximum charging currents that can be forced into the batteries $i_{bt1,ch}$ and $i_{bt2,ch}$ according to the manufacturer recommendations. By assuming that the mechanical losses can be neglected, the currents $i_{qs1limit}$ and $i_{qs2limit}$ can be calculated in a straightforward way as:

$$i_{qs1limit} = \frac{v_{bt,ch} \cdot i_{bt1,ch}}{\frac{3}{2} \overline{p} L_M \left(i_{ds1,rated} + i_{ds2,rated}\right) \omega_{rm,t0}} \quad (46)$$

$$i_{qs2limit} = \frac{v_{bt,ch} \cdot i_{bt2,ch}}{\frac{3}{2} \overline{p} L_M \left(i_{ds1,rated} + i_{ds2,rated}\right) \omega_{rm,t0}} \quad (47)$$

Numerous experimental tests have been conducted considering different values of $T_{e,demand}$ and $\omega_{rm,t0}$ as well as different values of SOC_{bt1} and SOC_{bt2} which imply different values of $i_{bt1,ch}$ and $i_{bt2,ch}$ i.e. different values of $i_{qs1limit}$ and $i_{qs2limit}$ from time to time. Within these constraints, the target is to select the suitable set of currents i_{qs1} e i_{qs2} which minimize the total losses.

The main experimental data of the "Braking" scenario, reported in Fig. 11, are obtained by:

i_{ds1}= $i_{ds1,rated}$=2 A, i_{ds2}= $i_{ds2,rated}$=0.8 A

$T_{e,demand}$=-5 Nm→ $i_{qs1}+i_{qs2}$≈-2.20 A

$\omega_{rm,t0}$=70 rad/s, $SOC_{bt1,t0}$=80% → $i_{bt1,ch}$≈-0.675 A → $i_{qs1limit}$≈-1.93 A

$\omega_{rm,t0}$=70 rad/s, $SOC_{bt2,t0}$=25% → $i_{bt2,ch}$≈-2.7 A → $i_{qs2limit}$≈-4.43 A

The relationships between q axis currents and battery limits have been determined by applying (17) and (14), whose correctness has been proved through the experimental tests depicted in the charts of Fig. 12 and Fig. 13.

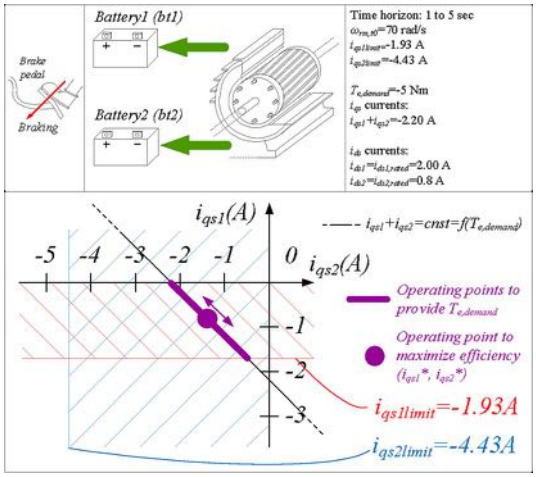

Fig. 11. Experimental test 1 - "Braking" scenario under investigation

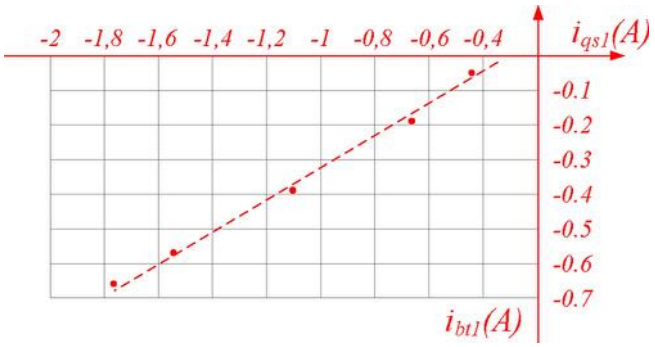

Fig. 12. Experimental data to validate the relationship (17) for the "Braking" scenario under investigation

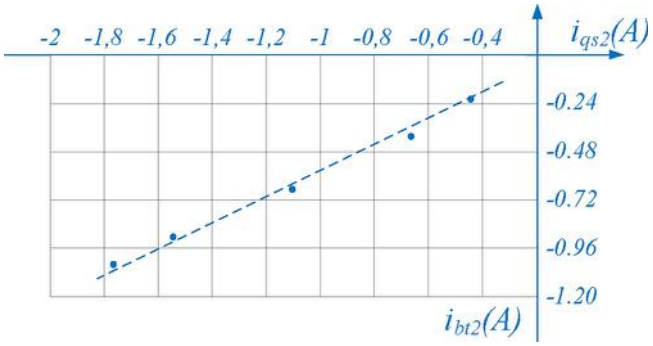

Fig. 13. Experimental data to validate the relationship (14) for the "Braking" scenario under investigation

Evaluating the total losses by means of (35), it can be plotted the chart of Fig. 14, where the total losses are represented as a function of i_{qs1} and i_{qs2} within the fixed constraints.

The minimum point (i.e. the maximum efficiency point) corresponds to a power loss of about 110 W, obtained with the set of currents calculated by solving (39):

$$i_{qs1}^{\Delta} = -1.42\,A, \quad i_{qs2}^{\Delta} = -0.78\,A \quad (48)$$

Alternatively, it can be exploited the proposed approach, providing a similar result:

$$\begin{cases} \dfrac{i_{qs1}}{i_{qs2}} \cong \dfrac{2 \cdot R_{sc} \cdot K_{sc}^2 + 3 \cdot R_{s2}}{2 \cdot R_{bt} \cdot K_{bt}^2 + 3 \cdot R_{s1}} = 1.6115 \\ i_{qs1} + i_{qs2} = -2.20 \end{cases} \quad (49)$$

$$i_{qs1}^* = -1.36\,A, \quad i_{qs2}^* = -0.84\,A$$

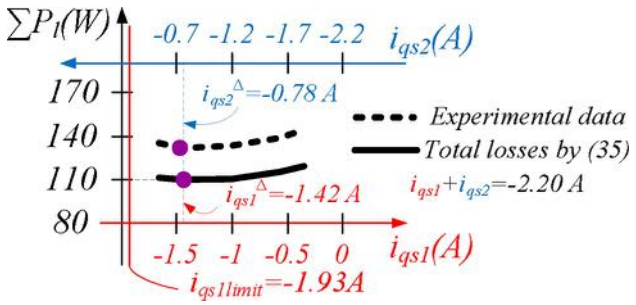

Fig. 14. Experimental test - Total losses curve for the "Braking" scenario under investigation.

The above result confirm that achieved by means of simulations. Compared to the total losses curve drawn by using (35), the experimental data curve has a similar shape but with an offset of about 20 W due to the power converters and mechanical losses not taken into account in (35). However, the position of the minimum losses point in the experimental data leads to q-axis current components very close to that provided by (39) i.e. i_{qs1}^{Δ}=-1.42 A, i_{qs2}^{Δ}=-0.78 A and to that provided by (41) i.e. i_{qs1}^{*}=-1.36 A, i_{qs2}^{*}=-0.84 A.

VI. Conclusions

This paper deals with the minimization of power losses in an integrated multi-drives (IMD) system used in hybrid electric vehicle (HEV) parallel drivetrains.

A suitable modeling for the induction machine, supercapacitors and batteries allows to evaluate in a simple but effective way the amount of the overall power losses.

An optimal vector control strategy is introduced and exploited to improve the energy efficiency considering the constraints assigned to each operating scenario.

References

[1] A. Castaings, W. Lhomme, R. Trigui and A.Bouscayrol, "Comparison of energy management strategies of a battery/supercapacitors system for electric vehicle under real-time constraints," in Applied Energy, vol. 163. New York, NY, USA: Elsevier, Feb. 2016, pp. 190–200.

[2] Z. Song, H. Hofmann, J. Li, J. Hou, X. Han and M. Ouyang, "Energy management strategies comparison for electric vehicles with hybrid energy storage system," in Applied Energy, vol. 134. New York, NY, USA: Elsevier, Dec. 2014, pp. 321–331.

[3] A. Tani, M. B. Camara and B. Dakyo, "Energy Management Based on Frequency Approach for Hybrid Electric Vehicle Applications: Fuel-Cell/Lithium-Battery and Ultracapacitors," IEEE Trans. Vehicular Technology, vol. 61, no. 8, pp. 3375-3386, Oct. 2012.

[4] J. O. Estima, A. J. M. Cardoso, "Efficiency Analysis of Drive Train Topologies Applied to Electric/Hybrid Vehicles," IEEE Trans. Vehicular Technology, vol. 61, no. 3, pp. 1021-1031, Mar. 2012.

[5] W. Shabbir, S. A. Evangelou, "Real-time control strategy to maximize hybrid electric vehicle powertrain efficiency," in Applied Energy, vol. 135. New York, NY, USA: Elsevier, Dec. 2014, pp. 512–522.

[6] J. Kessels, M. Koot, P. van den Bosch, D. Kok, "Online Energy Management for Hybrid Electric Vehicles," IEEE Trans. Vehicular Technology, vol. 57, no. 6, pp. 3428-3440, Nov. 2008.

[7] G. Scarcella, G. Scelba, M. Cacciato, A. Spampinato, M. M. Harbaugh, "Vector Control Strategy for Multidirectional Power Flow in Integrated Multidrives Starter-Alternator Applications," IEEE Trans. Industry Applications, vol. 52, no. 6, pp. 4816-4826, Dec. 2016.

[8] S. Castano, L. Gauchia and J. Sanz-Feito, "Effect of Packaging on Supercapacitors Strings Modeling: Proposal of Functional Unit Defined Around Balancing Circuit," IEEE Trans. Components, Packaging and Manufacturing Technology, vol. 3, no. 8, pp. 1390–1398, Aug. 2013.

[9] D. Rotenberg, A. Vahidi and I. Kolmanovsky, "Ultracapacitor Assisted Powertrains: Modeling, Control, Sizing, and the Impact on Fuel Economy," IEEE Trans. Control Systems Technology, vol. 19, no. 3, pp. 576-589, May 2011.

[10] S. M. Mousavi and M. Nikdel, "Various battery models for various simulation studies and applications," in Renewable and Sustainable Energy Reviews, vol. 32. New York, NY, USA: Elsevier, Apr. 2014, pp. 477–485.

[11] H. He, R. Xiong, H. Guo, and S. Li, "Comparison study on the battery models used for the energy management of batteries in electric ehicles," in Energy Conversion and Management, vol. 64. New York, NY, USA: Elsevier, Dec. 2012, pp. 113–121.

[12] M. Einhorn, F. V. Conte, C. Kral, and J. Fleig, "Comparison, selection, and parameterization of electrical batterymodels for automotive applications," IEEE Trans. Power Electronics, vol. 28, no. 3, pp. 1429–1437, Mar. 2013.

[13] M. Cacciato, G. Nobile, G. Scarcella, G. Scelba and A.G. Sciacca, "Energy management optimization in stand-alone power supplies using online estimation of battery SOC," in Proc. 2016 IEEE Power Electronics and Applications European Conf.

[14] G. L. Plett, "High-performance battery-pack power estimation using a dynamic cell model," IEEE Trans. Vehicular Technology, vol. 53, issue 5, pp. 1586-1593, Sep. 2004.

[15] M. Cugnet and B. Y. Liaw, "Effect of discharge rate on charging a lead-acid battery simulated by mathematical model," in Journal of Power Sources, vol. 196. New York, NY, USA: Elsevier, Apr. 2011, pp. 3414–3419.

[16] K. Marouani, M. Nesri, K. Nounou, "Rotor Flux Control with Copper Losses Reduction in a High Power Drive System," in Proc. 2016 IEEE International Power Electronics and Motion Control Conf.

[17] Ali M. Bazzi, P. T. Krein, "Review of Methods for Real-Time Loss Minimization in Induction Machines," IEEE Trans. Industry Applications, vol. 46, no. 6, pp. 2319-2328, Dec. 2010.

[18] A. Wang, Z. Ling, "Realization of Vector Control for Induction Motor Considering Iron Loss," in Proc. 2008 IEEE International Symposium on Intelligent Information Technology Application.

[19] S. Lim, K. Nam, "Loss-minimising control scheme for induction motors," IEEE Trans. Electric Power Applications, vol. 151, no. 4, pp. 385-397, July 2004.